Process Mineralogy for Critical Metals in Mineral Processing and Extractive Metallurgy

T. Grammatikopoulos

SGS Natural Resources, SGS Canada Inc., 185 Concession Street, Lakefield, Ontario, Canada K0L 2H0

Tassos.Grammatikopoulos@sgs.com

Abstract

We are mining minerals and not metals, thus critical metals are hosted by minerals, and assays may not be indicative of the mineral type and recovery. Because elements such as the rare earth elements (REE), lithium, niobium, gallium and scandium are distributed across several mineral hosts of differing chemistry, density, magnetic susceptibility and surface behaviour, a head grade alone carries almost no predictive information about how an ore will respond to grinding, flotation, magnetic separation or leaching. Process mineralogy resolves these parameters by quantifying the mineral matrix, mineral chemistry, grain size, and liberation and exposure characteristics of the ore, and by linking those measurements directly to metallurgical performance. This paper reviews the role of quantitative process mineralogy in the beneficiation and extraction of critical metals, using automated mineralogy (AMIN) by TIMA-X supported by XRD, EPMA, LA-ICP-MS and ToF-SIMS. Three case studies are presented: lithium pegmatites, where spodumene accounts for the great majority of contained Li and surface chemistry rather than liberation limits separation; REE deposits, where multiple REE hosts control both flotation selectivity and hydrometallurgical response; niobium carbonatites, where pyrochlore composition and particle exposure explain the gap between mineralogically predicted and achieved recoveries. Together they show that mineralogical data, acquired early and interpreted with metallurgical intent, reduces energy consumption, limits waste, and de-risks flowsheet development for the critical raw materials underpinning the energy transition.

Keywords: process mineralogy; automated mineralogy; critical metals; REE; lithium; niobium; geometallurgy; liberation

1. Introduction

Demand for the metals that underpin electrification and decarbonisation is rising faster than the supply base can comfortably respond. Under current stated policies, lithium demand is projected to grow roughly fivefold to 2040, while demand for REE and cobalt is expected to increase by 50–60% over the same period, driven largely by permanent magnets for electric vehicles and wind power (International Energy Agency 2025). Simultaneously, supply is geographically concentrated, project pipelines remain thin, and ore bodies currently entering development are lower in grade, finer-grained, and mineralogically more complex than their predecessors.

These challenges are not exclusively economic or geopolitical; they are fundamentally mineralogical. A niobium or REE assay informs the contained metal volume but does not specify whether that metal resides in a floatable, leachable, or refractory mineral. Ore deposits are inherently heterogeneous in composition, grain size, texture, and chemistry, and these attributes propagate directly into grinding energy, reagent selection, circuit configuration, and

final recovery. Process mineralogy operationalises this reality, combining state-of-the-art instrumentation to define geometallurgical domains, predict metallurgical behaviour, and optimise plant control across the entire mining cycle.

Process mineralogy is the discipline that makes that premise operational. It is the combination of experience, expertise and state-of-the-art instrumentation used as a quantitative tool to define geometallurgical domains, predict and troubleshoot metallurgical behaviour, forecast production, support process design and development, and maintain plant quality control and optimisation. Its value is realised across the whole mining cycle, from grade and volume at the exploration stage, through grade and tonnes in mine planning, to grade and recovery in the plant. Over the past two decades the field has matured alongside rapid improvements in quantitative analytical techniques, and it now sits at the core of modern geometallurgical workflows (Frenzel et al., 2023; Butcher et al., 2023).

This paper summarises the analytical toolbox, sets out the fundamental parameters that must be acquired for any critical metals project, and illustrates through case studies on Li, REE, and Nb how those parameters translate into decisions in mineral processing and extractive metallurgy.

2. The Analytical Toolbox

No single technique answers all of the questions a metallurgist asks. Process mineralogy is therefore an integrated approach in which each method contributes a specific piece of information, and in which the pieces are cross-validated against one another and against chemical assays.

Automated mineralogy (AMIN) using SEM-based platforms such as TIMA-X provides the quantitative backbone: modal mineral abundances, grain size distributions, textural relationships, and liberation, association and exposure statistics for the minerals of interest. Micro-riffled, representative sub-samples are mounted in resin and polished, and an X-ray spectrum is collected on a grid with pixel spacing adjustable between approximately 1 and 10 µm depending on the application. Mineral identification is based on the combination of back-scattered electron response and EDX spectra. The detection limit for a detectable element within a mineral is on the order of 0.5%, whereas the practical mineral detection limit is closer to 0.01%, an important distinction when the target phase is a trace REE or Nb mineral in a silicate or carbonate matrix.

X-ray diffraction supplies bulk mineralogy based on crystal structure, with a limit of detection of roughly 1–2% and no chemical information. It is indispensable where AMIN alone is ambiguous, most obviously in distinguishing spodumene from petalite. Electron microprobe analysis provides major-element mineral chemistry, Fe in spodumene, F in micas, individual REE in phosphates, silicates and fluorcarbonates, and LA-ICP-MS extends this to minor and trace elements such as Li, Cs, Rb and Ga. ToF-SIMS characterises the outermost surface layers of mineral grains and identifies organic, inorganic and molecular species: collectors, activators, depressants, oxidation products and contaminants carried by recycled process water.

Light elements are a well-known limitation. TIMA-X cannot detect Be, Li or B directly, but the minerals hosting them can still be classified reliably from their Al/Si ratios and validated against XRD, EPMA and LA-ICP-MS. Sample preparation matters as much as the measurement: gravity settling in the mount must be prevented, replicate grain mounts prepared, and reproducibility verified between them. Quality assurance rests on comparing TIMA-X-derived

calculated assays against actual chemical assays, with agreement within roughly 10% treated as acceptable. Two-dimensional sectioning also introduces stereological bias in apparent grain size, which should be acknowledged when liberation data are used quantitatively (Butcher et al., 2023).

3. The Fundamental Parameters

Four measurements do most of the work in any critical metals study.

3.1. Mineral matrix and correct identification

Critical elements are almost never confined to a single host. In pegmatites, Li occurs in spodumene, petalite, amblygonite, zinnwaldite, lepidolite and Li-phosphates, all showing extensive solid solution; in REE deposits the metal is partitioned among phosphates, fluorcarbonates, silicates and oxides. Correct identification matters for three reasons: not all minerals are recovered or rejected by the same process; the metal is distributed across several phases in different proportions; and some minerals are deleterious in themselves (thorite) or carry penalty elements such as U and Th. Geochemical analysis alone cannot resolve any of this.

Table 1 presents the mineral mass distribution of four composite samples representing four different pegmatite domains. The data show variations in mineral grades. The variation in spodumene that carries most of Li, muscovite and Li phosphates which can also carry significant Li are highlighted. On the other hand, K-feldspars that can carry Rb and Cs also vary among the samples. Table 2 presents the mineral mass distribution of two composite samples from the same REE ore. COMP 1 hosts mainly F-C REM and burbankite and COMP 2 kukharenkoite and ancylite. This will have a significant impact on the final REE grade as fluorcarbonate rare earth minerals (F-C-REM) and monazite host significantly more REE than burbankite, kukharenkoite and ancylite.

Table 1. Modal mineralogy by Calculated Head for a pegmatite spodumene ore

Mineral/Sample	Peg B	Peg C	Peg D	Peg E
Spodumene	14.7	23.3	19.7	11.9
Petalite	0.88	0.70	1.99	1.83
Cookeite	0.20	0.06	0.12	0.04
Beryl	0.02	0.02	0.23	0.37
Tantalite	0.00	0.00	0.01	0.02
Columbite	0.01	0.00	0.01	0.03
Pollucite	0.00	0.00	0.00	0.00
Quartz	31.8	29.5	24.8	31.3
K-feldspars	12.6	14.9	5.34	14.7
Albite	32.1	25.1	35.9	28.0
Muscovite	6.10	5.20	3.82	8.79
Lepidolite	0.09	0.04	0.07	0.04
Tourmaline	0.15	0.10	0.67	0.18
Pyroxene/Amphibole	0.01	0.01	1.44	0.02
Epidote	0.07	0.06	0.96	0.14
Biotite	0.30	0.24	1.51	0.73
Chlorite	0.03	0.01	2.08	0.08
Garnets	0.08	0.01	0.12	0.05
Carbonates	0.05	0.02	0.15	0.02
Titanite	0.02	0.01	0.08	0.02
Apatite	0.42	0.28	0.47	0.31
Fluorite	0.00	0.00	0.01	0.00
Phosphates (Li)	0.23	0.34	0.27	1.16
Fe-(Ti)-Oxides	0.06	0.06	0.08	0.09
Gahnite	0.06	0.00	0.00	0.01
Sulphides	0.03	0.01	0.03	0.03
Other	0.04	0.03	0.06	0.05
Total	100	100	100	100

Table 2. Modal mineralogy by size fraction of a REE ore

Sample	**COMP 1**					**COMP 2**				
Fraction	**Combined**	**+45 um**		**-45 um**		**Combined**	**+45 um**		**-45 um**	
Mass Size Distribution (%)	100.0	45.2		54.8		100.0	54.2		45.8	
Sample/Fraction	Sample	Sample	Fraction	Sample	Fraction	Sample	Sample	Fraction	Sample	Fraction
Bastnasite	1.49	1.55	0.70	1.43	0.79	0.01	0.00	0.00	0.01	0.00
Synchysite/Parisite	1.05	0.81	0.37	1.25	0.69	0.09	0.07	0.04	0.12	0.06
Monazite	1.43	1.04	0.47	1.76	0.97	0.11	0.05	0.03	0.17	0.08
Burbankite	2.62	2.73	1.23	2.53	1.39	0.02	0.02	0.01	0.03	0.01
Cerite	0.00	0.00	0.00	0.00	0.00	0.01	0.00	0.00	0.01	0.00
Kukharenkoite	0.41	0.34	0.16	0.46	0.25	1.74	1.33	0.72	2.22	1.02
Kukharenkoite(Oxidized)	0.13	0.06	0.03	0.18	0.10	0.91	0.81	0.44	1.04	0.47
Ancylite	1.81	2.10	0.95	1.57	0.86	1.09	1.08	0.59	1.09	0.50
Pyrochlore	0.02	0.01	0.01	0.02	0.01	0.01	0.01	0.00	0.02	0.01
Other REM	0.00	0.00	0.00	0.00	0.00	0.00	0.00	0.00	0.00	0.00
Calcite	4.09	3.28	1.48	4.76	2.61	2.86	2.59	1.40	3.18	1.46
Siderite	20.1	24.1	10.9	16.8	9.22	26.5	31.1	16.9	21.2	9.69
Ankerite	37.2	36.8	16.6	37.5	20.6	17.0	17.1	9.25	16.9	7.72
Dolomite	11.9	11.5	5.21	12.2	6.66	1.59	1.38	0.75	1.83	0.84
Siderite/Ankerite(Ba)	0.07	0.07	0.03	0.07	0.04	0.19	0.17	0.09	0.22	0.10
Olekminkite	0.01	0.01	0.00	0.02	0.01	0.15	0.10	0.05	0.21	0.10
Alstonite	0.08	0.08	0.04	0.08	0.04	9.39	10.3	5.60	8.28	3.79
Strontianite	0.28	0.30	0.14	0.27	0.15	2.14	1.95	1.06	2.36	1.08
Barite	2.57	2.32	1.05	2.77	1.52	21.8	20.3	11.0	23.6	10.8
Anandite	0.00	0.00	0.00	0.01	0.00	0.08	0.01	0.01	0.16	0.07
Barioferrite	0.19	0.07	0.03	0.29	0.16	0.28	0.03	0.02	0.58	0.26
Thorite	0.05	0.03	0.01	0.06	0.04	0.03	0.02	0.01	0.04	0.02
Quartz	0.32	0.37	0.17	0.28	0.15	0.29	0.31	0.17	0.26	0.12
Feldspars	2.82	2.92	1.32	2.74	1.50	2.19	2.19	1.19	2.20	1.01
Amphibole/Pyroxenes	1.44	0.61	0.28	2.12	1.16	3.15	2.39	1.30	4.05	1.86
Chlorites	0.15	0.12	0.06	0.17	0.09	0.09	0.05	0.03	0.13	0.06
Micas	0.03	0.04	0.02	0.03	0.01	0.15	0.18	0.10	0.11	0.05
Pellyite	0.18	0.06	0.03	0.27	0.15	0.10	0.03	0.02	0.18	0.08
Other Silicates	0.03	0.02	0.01	0.03	0.02	0.10	0.08	0.05	0.12	0.05
Apatite	3.32	2.99	1.35	3.59	1.97	0.66	0.56	0.30	0.78	0.36
Sulphides	3.29	3.89	1.76	2.79	1.53	2.46	2.39	1.29	2.55	1.17
Fe-Oxides	2.87	1.69	0.76	3.84	2.10	4.75	3.40	1.84	6.35	2.91
Rutile	0.01	0.01	0.00	0.00	0.00	0.01	0.01	0.00	0.02	0.01
Other Minerals	0.07	0.04	0.02	0.10	0.05	0.05	0.03	0.02	0.07	0.03
Total	100.0	100.0	45.2	100.0	54.8	100.0	100.0	54.2	100.0	45.8

3.2. Mineral chemistry and metal deportment

Metal deportment, the distribution of an element among its host minerals, calculated from mineral mass and mineral chemistry, determines the theoretical ceiling on recovery and identifies where losses and by-products will occur. It also drives surface behaviour: variations in Fe content within pyrochlore, or F content distinguishing lepidolite from muscovite, change flotation response even though the mineral name does not change. Chemical composition of REE can also vary widely in both major and trace elements (e.g., Gillerman et al., 2025). EPMA and LA-ICP-MS of REE minerals was conducted on monazite, F-C-REM and other minerals. The results indicate a revealing picture. Monazite-1 averages 7.73 wt% Nd_2O_3, Monazite-2 21.88wt% and Monazite-3 37.60 wt% (Table 3). Similar trends are observed in F-C-REM in the same samples.

3.3. Liberation, association and exposure

Liberation classes are defined here by surface exposure: pure (100%), free (≥95%), liberated (≥80% but <95%), middlings (a mineral of interest with gangue), and locked. Exposure, rather than area percent liberation, is the parameter that governs flotation, since a bubble can only attach to exposed surface. Association identifies which gangue minerals must be broken away and therefore which comminution or regrind duty is required.

Table 3. Monazite Chemistry from three different domains within an REE ore

Mineral	Oxide/Element	Monazite -1			Monazite -2			Monazite-3		
Analytical Method	Range	Min	Max	Avg.	Min	Max	Avg.	Min	Max	Avg.
EPMA (wt%)	Nb2O5	n/d	0.07	0.01	n/d	0.08	0.02	n/d	0.11	0.01
	Ta2O5	n/d	0.15	0.01	n/d	0.09	0.02	n/d	0.07	0.01
	SiO2	n/d	n/d	n/d	n/d	4.15	0.20	n/d	1.64	0.05
	TiO2	n/d	n/d	n/d	n/d	0.05	0.00	n/d	n/d	n/d
	PbO	n/d	n/d	n/d	n/d	n/d	n/d	n/d	0.02	0.00
	ThO2	0.12	2.20	0.77	0.10	1.30	0.55	0.24	0.86	0.49
	UO2	n/d	0.09	0.02	n/d	0.06	0.01	n/d	n/d	n/d
	Al2O3	n/d	n/d	n/d	n/d	10.71	0.76	n/d	1.45	0.05
	Y2O3	n/d	0.21	0.02	n/d	0.68	0.23	0.38	1.30	0.79
	La2O3	22.64	27.04	24.68	0.79	26.66	13.65	2.25	3.94	3.06
	Ce2O3	32.12	35.08	33.60	5.78	34.50	23.74	13.80	16.92	15.75
	Pr2O3	1.78	2.53	2.08	0.97	6.08	3.28	4.68	5.74	5.28
	Nd2O3	6.45	8.58	7.73	0.00	40.31	21.88	35.06	40.66	37.60
	Sm2O3	0.22	0.61	0.41	n/d	6.47	2.72	4.69	5.78	5.12
	Eu2O3	0.09	0.28	0.19	n/d	1.16	0.50	0.55	0.98	0.75
	Gd2O3	n/d	0.43	0.17	n/d	2.03	0.62	1.16	1.77	1.44
	Tb2O3	n/d	0.09	0.02	n/d	0.07	0.01	n/d	n/d	n/d
	Dy2O3	n/d	0.14	0.03	n/d	0.28	0.09	0.08	0.52	0.29
	Ho2O3	n/d	0.13	0.02	n/d	0.12	0.03	n/d	0.20	0.05
	Er2O3	n/d	0.04	0.01	n/d	0.06	0.02	n/d	0.16	0.06
	Tm2O3	n/d	0.09	0.01	n/d	0.10	0.01	n/d	0.09	0.02
	Yb2O3	n/d	0.05	0.01	n/d	0.08	0.02	n/d	0.07	0.03
	Lu2O3	n/d	0.06	0.01	n/d	0.08	0.01	n/d	0.04	0.00
	FeO	n/d	n/d	n/d	n/d	1.36	0.13	n/d	n/d	n/d
	MnO	n/d	0.05	0.02	n/d	0.08	0.03	n/d	0.11	0.06
	MgO	n/d	n/d	n/d	n/d	5.97	0.29	n/d	n/d	n/d
	CaO	0.04	0.54	0.12	0.03	1.26	0.30	0.07	0.54	0.17
	SrO	0.02	1.28	0.28	n/d	0.27	0.09	n/d	0.11	0.02
	BaO	n/d	0.04	0.00	n/d	0.16	0.02	n/d	0.04	0.00
	Na2O	n/d	n/d	n/d	n/d	0.02	0.00	n/d	n/d	n/d
	P2O5	29.53	30.78	30.16	26.68	30.64	29.41	28.35	30.12	29.54
	SO3	n/d	0.12	0.02	n/d	0.99	0.27	0.01	0.19	0.07
	F	n/d	n/d	n/d	n/d	0.07	0.00	n/d	n/d	n/d
	CO2	n/d	n/d	n/d	n/d	n/d	n/d	n/d	n/d	n/d
	O	n/d	0.00	0.00	n/d	0.00	0.00	n/d	0.00	0.00
	H2O	n/d	n/d	n/d	n/d	n/d	n/d	n/d	n/d	n/d
	TOTAL	99.21	101.39	100.40	90.49	103.12	98.91	99.81	101.81	100.71
LA-ICP-MS (ppm)	Ga	1184.9	1385.7	1280.5	940.6	1634.1	1248.1	1220.7	2001.2	1751.6
	Ge	983.9	1417.8	1218.9	905.7	5326.9	2788.6	3699.7	5909.2	5045.7

3.4. Grain size

Grain size sets the achievable liberation and hence the grind target. It also defines the lower bound of practical recovery, because material ground below roughly 10-20 μm is increasingly lost to entrainment and to the slimes fraction regardless of how well it is liberated.

Taken together these parameters allow geometallurgical domains to be defined, spatially distinct zones with consistent geological, mineralogical and textural properties that predict similar processing behaviour. Domaining in turn supports selective mining and blending, targeting high-grade or better-liberated zones and leaving low-value material in place, which reduces the tonnage mined, hauled and ground per unit of metal produced.

4. Case Studies

4.1. Lithium pegmatites: when liberation is not the problem

Hard-rock lithium extraction is more complex and more energy intensive than brine production, and more than thirty Li-bearing minerals are known although only five are mined at scale. XRD is used first to establish whether spodumene and petalite occur together or in separate domains, because that distinction alone determines the mine plan: the Li grade reflects all Li minerals, but the flowsheet cannot (e.g., Grammatikopoulos et al., 2021; Aylmore et al., 2018; Gibson et al., 2017).

AMIN coupled with LA-ICP-MS was used to calculate Li, Cs and Rb deportment in a granitic pegmatite. Spodumene accounted for 79-95% of contained Li (Figure 1). The Li-bearing micas and phosphates were both low in abundance

and low in Li concentration, which favours a simple spodumene concentrate with minimal losses in the three samples but not in the fourth. The common assumption that Li concentration in spodumene is constant is not supported by the data: LA-ICP-MS shows appreciable internal variability reflecting zoning and alteration, and this variability propagates directly into the mineralogically limited grade–recovery relationship. Cs and Rb, by contrast, reported almost entirely to micas and K-feldspars and represent a potential by-product stream rather than a contaminant.

The more instructive result concerned a circuit in which liberation was adequate and recovery was nonetheless poor. Spodumene was reporting to the mica (gangue) circuit while albite floated in the spodumene circuit, depressing both recovery and final concentrate grade. ToF-SIMS analysis of grains from multiple streams, comparing normalised median intensities of collector fragments, showed that the collectors were not selective towards a specific mineral. The constraint was surface chemistry, not texture (Di Feo et al., 2025). This is a general point: where liberation data cannot explain a metallurgical result, surface analysis usually can, and recent work confirms that both the grinding environment and the conditioning regime materially alter spodumene surface composition and flotation response (Opoku et al., 2025).

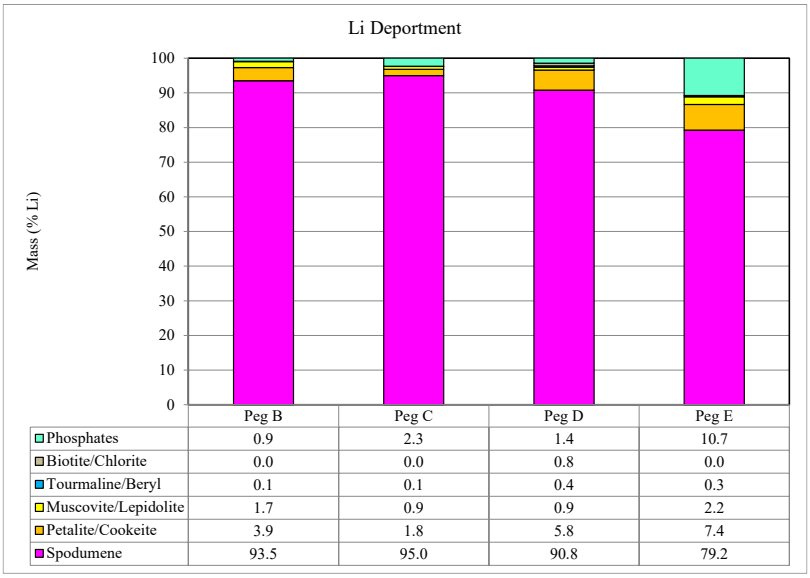

	Peg B	Peg C	Peg D	Peg E
Phosphates	0.9	2.3	1.4	10.7
Biotite/Chlorite	0.0	0.0	0.8	0.0
Tourmaline/Beryl	0.1	0.1	0.4	0.3
Muscovite/Lepidolite	1.7	0.9	0.9	2.2
Petalite/Cookeite	3.9	1.8	5.8	7.4
Spodumene	93.5	95.0	90.8	79.2

Figure 1: Li deportment in a granitic pegmatite, calculated from AMIN modal mineralogy and LA-ICP-MS mineral chemistry

4.2. REE deposits: multiple hosts, two very different problems

The type, chemistry and textural complexity of REE minerals vary widely between and within deposits, and flowsheets must reflect the matrix, the primary and secondary textures and the mineral chemistry in addition to liberation. REE phosphates and silicates float differently, and rejection of either one produces low REE grades in the concentrate.

Speciation by AMIN also supports ore zonation, since deposits can be mapped on ratios of heavy to light REE minerals, or of silicates to phosphates to fluorcarbonates to oxides (Grammatikopoulos et al., 2013).

Deportment frequently overturns the initial geological interpretation. In one IOCG-affiliated deposit with TREO grades of approximately 2%, discrete REE minerals were too sparse to account for the assay; apatite was found to host 6.2% TREE+Y and was the principal carrier, which changes the flowsheet entirely (Grammatikopoulos et al., 2026). In another, fergusonite and zircon accounted for most of the HREE while monazite, allanite, synchysite and bastnäsite carried the LREE in decreasing order, a distribution that has direct consequences for which products can be marketed.

As shown above (Table 2) two composite samples from the same REE ore yield in COMP 1 mainly F-C REM and burbankite and in COMP 2 kukharenkoite and ancylite. While the liberation, grain size, flotation response will control the recovery of the minerals, the final REE grade of the concentrate will be controlled by the proportions of type of REE minerals. F-C-REM and monazite host significantly more REE than burbankite, kukharenkoite and ancylite. Therefore, a lower REE grade concentrate is expected in COMP 2. Furthermore, the concentrate in COMP 2 will have to be treated for the higher Ba and Sr concentrations in addition to other gangue elements.

Liberation controls the grind target. For a carbonatite composite at a P_{80} of 212 µm, calculated monazite liberation was low at approximately 41%, increased markedly below 106 µm, and reached about 60% in the -25 µm fraction (Figure 2). Grinding below 106 µm is therefore required if monazite is to be recovered, and particle maps distinguish well-exposed monazite that is theoretically recoverable from poorly exposed grains locked with carbonates that are not. The counter-pressure is that monazite is brittle, so over-grinding pushes it into the slimes where it is lost. Mineralogy defines the window between the two.

Mineralogy is equally decisive downstream. TIMA-X examination of a flotation concentrate and three leach residues, gangue leach, caustic crack/water wash, and acid leach, tracked the fate of each phase through the hydrometallurgical circuit. The concentrate comprised synchysite/parisite (61%), monazite (approximately 21%) and carbonates (14%, dolomite and ankerite). Roughly 10% of the carbonates were removed in the gangue leach. The caustic crack residue showed that considerable monazite had been cracked, leaving REE dominated by fluorcarbonate phases, while acid leaching removed the fluorcarbonates but generated a hydrated monazite. Closer examination revealed monazite grains only partially dissolved and rimmed by phosphorus-depleted REE compounds resembling bastnäsite/synchysite/parisite, and by a hydrated monazite depleted in P and enriched in Ce and La. Residue mineralogy of this kind explains extraction shortfalls that solution chemistry alone cannot.

An example of deportment of selected REE is shown in Figure 3. It is critical to note that Y for example is split between fergusonite and zircon. LREE are controlled by F-C-REM and monazite.

4.3. Niobium carbonatites: explaining the gap between prediction and plant

A large sample set from a niobium carbonatite was analyzed to determine the Nb-bearing minerals and their liberation. Pyrochlore is the principal Nb host, but its composition varies from Ba-rich to Ba-poor, with significant variation in Fe, U and Th between samples. That compositional variability affects both flotation response and achievable Nb grade, a result consistent with independent surface-chemistry work showing that recovery favours lower-Fe pyrochlore

varieties, that cationic collector species preferentially report to Fe-poor grains, and that higher-Fe pyrochlore is preferentially surface-oxidised (Chehreh Chelgani, 2013).

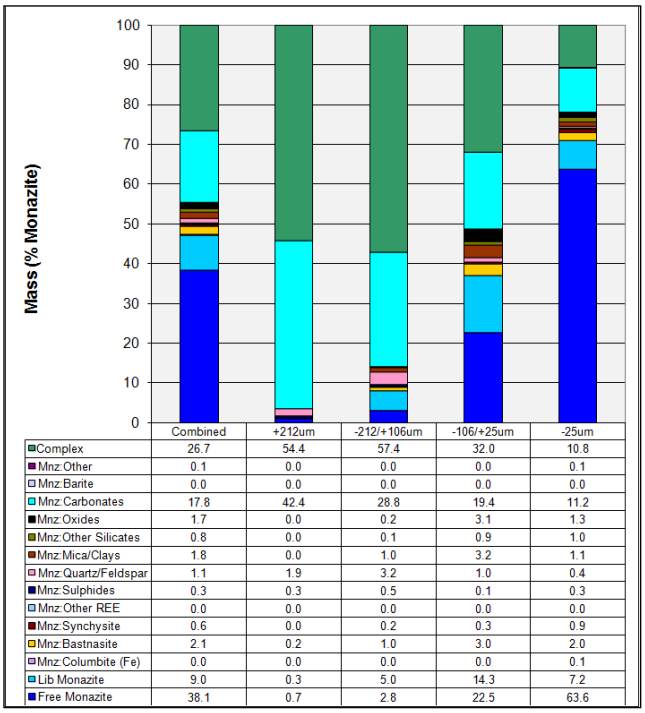

	Combined	+212um	-212/+106um	-106/+25um	-25um
Complex	26.7	54.4	57.4	32.0	10.8
Mnz:Other	0.1	0.0	0.0	0.0	0.1
Mnz:Barite	0.0	0.0	0.0	0.0	0.0
Mnz:Carbonates	17.8	42.4	28.8	19.4	11.2
Mnz:Oxides	1.7	0.0	0.2	3.1	1.3
Mnz:Other Silicates	0.8	0.0	0.1	0.9	1.0
Mnz:Mica/Clays	1.8	0.0	1.0	3.2	1.1
Mnz:Quartz/Feldspar	1.1	1.9	3.2	1.0	0.4
Mnz:Sulphides	0.3	0.3	0.5	0.1	0.3
Mnz:Other REE	0.0	0.0	0.0	0.0	0.0
Mnz:Synchysite	0.6	0.0	0.2	0.3	0.9
Mnz:Bastnasite	2.1	0.2	1.0	3.0	2.0
Mnz:Columbite (Fe)	0.0	0.0	0.0	0.0	0.1
Lib Monazite	9.0	0.3	5.0	14.3	7.2
Free Monazite	38.1	0.7	2.8	22.5	63.6

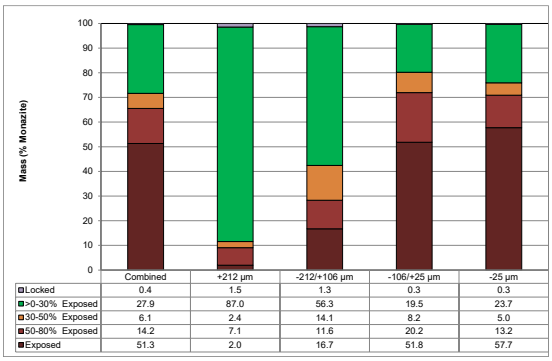

	Combined	+212 µm	-212/+106 µm	-106/+25 µm	-25 µm
Locked	0.4	1.5	1.3	0.3	0.3
>0-30% Exposed	27.9	87.0	56.3	19.5	23.7
30-50% Exposed	6.1	2.4	14.1	8.2	5.0
50-80% Exposed	14.2	7.1	11.6	20.2	13.2
Exposed	51.3	2.0	16.7	51.8	57.7

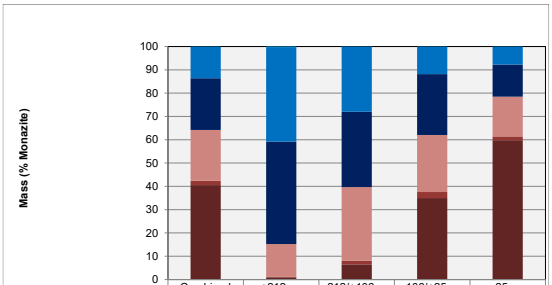

	Combined	+212um	-212/+106um	-106/+25um	-25um
Non-Recoverable-Locked	0.1	0.3	0.1	0.1	0.0
Non Recoverable - Exposed	13.6	40.6	27.9	11.8	7.7
Mnz:Carb/Ox/Sil	22.1	43.9	32.4	26.1	13.8
Recoverable	21.8	14.1	31.6	24.5	17.0
Mnz:REM	1.9	0.2	1.5	2.6	1.6
Lib Monazite	40.5	1.0	6.5	35.0	59.8

Figure 2: (left) Monazite liberation and association, and (right) exposure and recoverability by size fraction for a carbonatite composite at P_{80} 212 µm

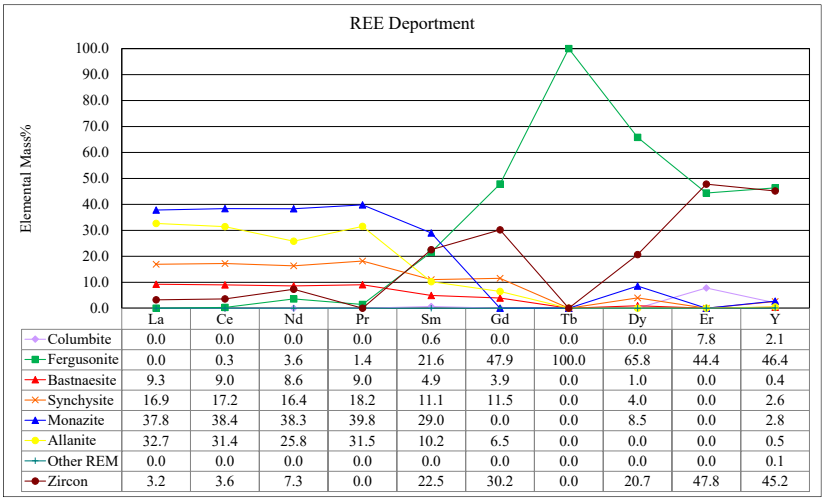

	La	Ce	Nd	Pr	Sm	Gd	Tb	Dy	Er	Y
Columbite	0.0	0.0	0.0	0.0	0.6	0.0	0.0	0.0	7.8	2.1
Fergusonite	0.0	0.3	3.6	1.4	21.6	47.9	100.0	65.8	44.4	46.4
Bastnaesite	9.3	9.0	8.6	9.0	4.9	3.9	0.0	1.0	0.0	0.4
Synchysite	16.9	17.2	16.4	18.2	11.1	11.5	0.0	4.0	0.0	2.6
Monazite	37.8	38.4	38.3	39.8	29.0	0.0	0.0	8.5	0.0	2.8
Allanite	32.7	31.4	25.8	31.5	10.2	6.5	0.0	0.0	0.0	0.5
Other REM	0.0	0.0	0.0	0.0	0.0	0.0	0.0	0.0	0.0	0.1
Zircon	3.2	3.6	7.3	0.0	22.5	30.2	0.0	20.7	47.8	45.2

Figure 3: Complex REE deportment

Theoretical grade-recovery curves generated from AMIN data were compared with actual metallurgical performance. Recoveries fell between 60% and 80% of contained Nb_2O_5 (Figure 4). Where the mineralogically predicted grade exceeded that achieved, three loss mechanisms were identified: fine-grained pyrochlore below 20 µm lost by entrainment; coarse particles with poor surface exposure; and coarse liberated grains for which the reagent scheme was less effective. Each has a specific remedy, longer flotation retention time for the fines, flash flotation for coarse liberated pyrochlore, and regrinding of coarse middlings to increase exposure. Other samples showed close agreement between theoretical and metallurgical values; in those, pyrochlore was 10–20 µm coarser and the middlings carried pyrochlore with higher surface exposure.

Whether 60-80% Nb_2O_5 recovery is acceptable is a question mineralogy informs but does not answer alone. Pyrochlore flotation has intrinsic limitations, and 100% recovery at high grade is not achievable on any project (Gibson, 2016). Where Nb grades are high, 60-80% may represent the practical limit for a fine-grained or complexly intergrown ore; finer grinding and better selectivity could lift it, at a cost. For a low-grade, high-tonnage, low-strip deposit, a lower recovery may still be economic. The mineralogical data define what is physically possible; the economics decide what is worth doing.

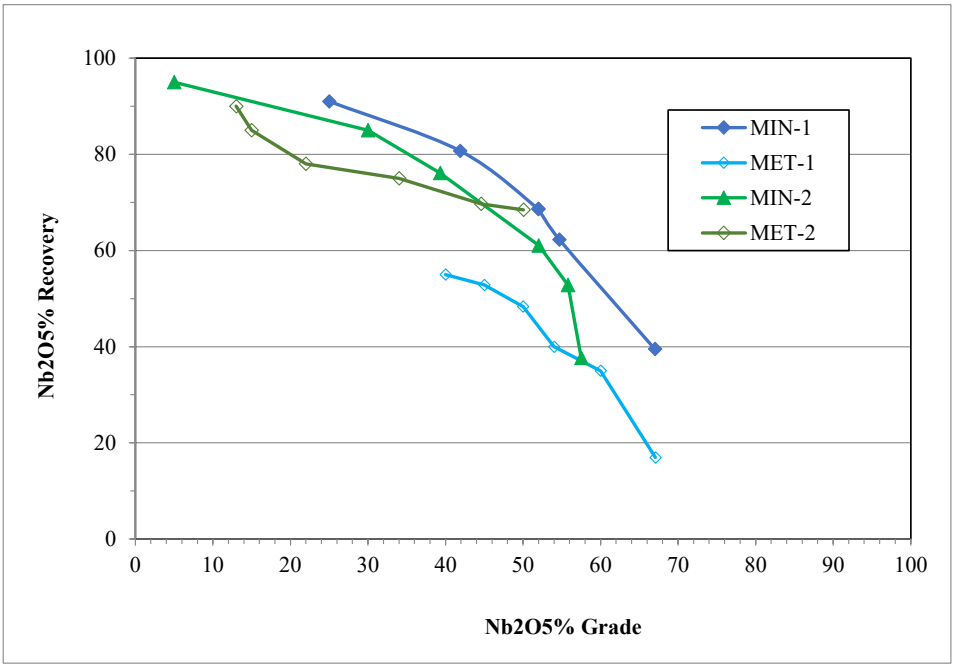

Figure 4: liberation/association, exposure and recoverability

5. Energy, Waste and the Circular Economy

Comminution is the single largest energy consumer on most mine sites, accounting for a substantial share of site electrical energy and, for copper and gold ores alone, an estimated 0.2% of global electricity consumption (Ballantyne

and Powell, 2014). Any decision that avoids unnecessary grinding is therefore a decision with a measurable carbon and cost consequence. Mineralogy is what makes such decisions defensible.

Liberation-versus-particle-size curves determine primary and secondary grind targets directly, and the overall mineral assemblage and textural association indicate how much energy will be required to grind material from a given block. The objective is the necessary degree of fineness for liberation, not the maximum achievable, and the REE case above illustrates the penalty for overshooting, where over-grinding of brittle monazite moves metal into the slimes and out of the concentrate. Identifying gangue mineralogy up front also directs the choice of separation route: Fe-oxides may indicate magnetic separation, carbonates and silicates may indicate flotation, and clays that raise pulp viscosity or minerals that react with process water can be designed around rather than discovered during commissioning.

Better liberation and better-informed separation produce higher-grade concentrates and smaller tailings volumes. Characterising the mineralogy of those tailings is equally important, both for environmental risk, the presence of Th and U in REE deposits being the obvious case, and for future valorisation, since residual critical metal contents in historical tailings are increasingly viable secondary resources. Particle-based approaches to tailings characterisation now allow reprocessing potential to be assessed with the same rigour as a primary resource (Blannin et al., 2024). Precise phase identification also permits more specific reagent selection, reducing both cost and discharge.

6. From Description to Prediction

Process mineralogy has historically been descriptive, delivered after the metallurgical result and used to explain it. The direction of travel is towards prediction, and three developments are converging.

The first is particle-based modelling. Rather than treating a stream as a bulk composition, separation can be modelled at the resolution of individual complex particles using automated mineralogy data and machine learning, allowing recovery to be forecast from measured particle properties rather than inferred from batch tests (Pereira et al., 2023). The second is the automation of mineral classification itself, where machine learning applied to EDX spectra improves discrimination of fine-grained and mixed phases and can flag anomalous spectra that rule-based classification would silently misassign (Su et al., 2025), a persistent difficulty for REE minerals with overlapping spectral signatures. The third is the extension of geometallurgical thinking earlier in the project lifecycle, supported by drill-core scanning and multi-scale characterisation, so that mineralogical constraints are known during scoping rather than during feasibility (Tusa et al., 2025).

None of this displaces the mineralogist. Models are only as good as the mineral identifications and mineral chemistry that feed them, and the interpretation of what a liberation curve or a deportment table means for a specific flowsheet remains a matter of judgement built on experience. What these developments do change is the speed and confidence with which mineralogical data can be turned into a metallurgical forecast.

Figure 5 presents the distribution of minerals and selected oxides from various products from a pilot plant. Given the fact that REE can be hosted in different minerals AMIN analysis can resolve the REE mineral, liberation and grain size to determine the cause of losses. Therefore, an evaluation of entrainment, liberation, grain size, and type of REE mineral loss can inform the flowsheet development. Mass and oxide balances made the losses explicit: AMIN

identified allanite and monazite as responsible for the majority of LREE losses, allanite because it is a silicate and was being rejected, monazite because it was lost in the slimes. That information was fed back into flowsheet development to target improved flotation selectivity through changes to reagents and circuit arrangement (e.g., Chehreh Chelgani, 2013).

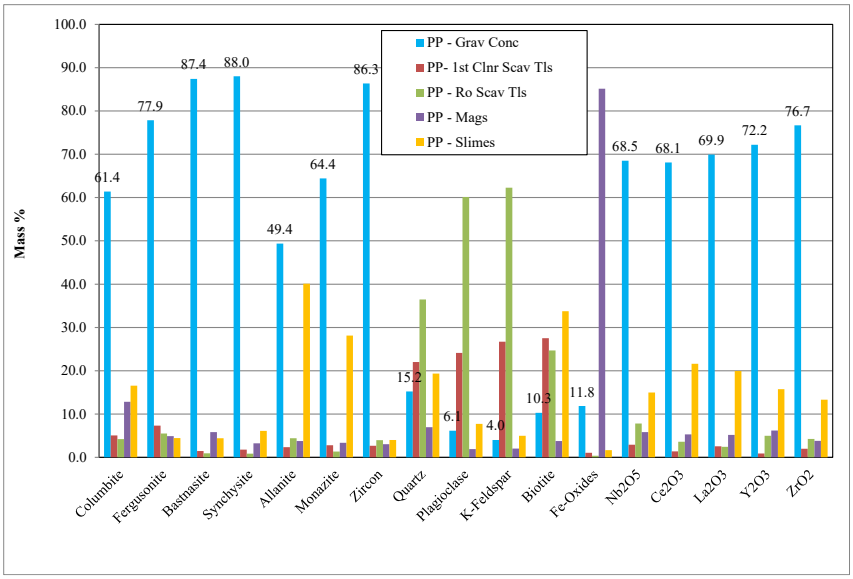

Figure 5: Mineral and corresponding REO for various products from a pilot plant

7. Metallurgical implications

The mineralogical deportment of an example rare earth element (REE) deposit exhibits a sharp bifurcation between heavy (HREE) and light (LREE) rare earth elements across multiple disparate mineral classes (Figure 3). This distribution dictates the flowsheet complexity, operating and capital expenditures (OPEX/CAPEX), and absolute recovery ceilings for the project.

Hosting 100% of the terbium and 65.8% of the dysprosium, fergusonite is the primary driver of the project's Net Smelter Return (NSR). Maximizing recovery requires targeted high-gradient magnetic separation, gravity concentration (leveraging its 5.5–5.8 specific gravity), or specialized flotation (Jordens et al., 2014). High fergusonite recovery is the single most critical economic factor and may also yield secondary niobium/tantalum byproduct credits. Conversely, zircon traps 20.7% of the dysprosium and over 45% of the yttrium. Because zircon resists standard acid-bake or direct leaching, extracting REEs from this phase requires highly energy-intensive caustic fusion (>600°C) or plasma processing (da Silva et al., 2012), which is uneconomic for REE extraction alone. This establishes a rigid theoretical recovery ceiling, rendering these specific HREE fractions metallurgically unrecoverable within conventional processing circuits.

Allanite hosts approximately 30% of the Nd-Pr basket but presents severe downstream processing challenges. Its surface properties mimic common silicate gangue (e.g., feldspars, pyroxenes), severely complicating selective bulk flotation. Furthermore, allanite dissolves incongruently in acid, causing silica gelation that blinds solid-liquid separation equipment (thickening and filtration) and drastically increases hydrometallurgical OPEX (Xiao and Zhang, 2024). The remaining Nd-Pr value is split between monazite (~38-40%) and (F-C-REM, ~25-27%). Monazite requires aggressive, high-temperature acid cracking (200-250°C) and introduces strict environmental permitting and tailings neutralization requirements due to associated thorium and uranium. While F-C-REM allow for milder leaching conditions, the stoichiometric calcium in synchysite drives high acid consumption and precipitates problematic gypsum within sulfuric acid circuits.

The distribution of pay metals across phosphates, silicates, F-C-REM, and complex oxides precludes the use of a single concentration stage. Inherent variances in physical densities, points of zero charge (PZC), and collector adsorption kinetics necessitate a complex, multi-stage hybrid circuit. A typical configuration requires rigorous desliming followed by gravity and magnetic separation for fergusonite and zircon, trailed by sequential or bulk selective flotation for the F-C-REM and monazite. This hybrid approach significantly increases the plant footprint, water handling costs, and overall capital intensity, while generally capping combined circuit recoveries at 60–70%.

Ultimately, economic feasibility for this deposit requires modeling phase-specific metallurgical recoveries rather than relying on whole-rock head assays. Project viability hinges on optimizing fergusonite recovery in the physical beneficiation circuit while successfully upgrading monazite and F-C-REM into a viable concentrate without entraining intolerable levels of silica-forming allanite.

The hydrometallurgical extraction of REEs is heavily dictated by the specific mineralogical deportment of the ore, requiring tailored conditions for different mineral classes. For refractory phosphate hosts such as monazite, standard extraction relies on a high-temperature (180-250°C) sulfuric acid bake-and-leach. This aggressive cracking process converts the REE-phosphates into water-soluble sulfates, allowing for subsequent recovery alongside radioactive elements like thorium and uranium (Berry et al., 2018). The efficiency of this acid baking process is highly sensitive to the surrounding gangue mineralogy. Notably, the presence of iron oxide and hydroxide gangue during the bake enhances the overall dissolution of REEs and thorium by preferentially forming insoluble iron sulfate-polyphosphate phases, which prevents the reprecipitation of REE-polyphosphates (Demol et al., 2022).

Conversely, fluorocarbonate minerals like bastnäsite and synchysite are typically processed through roasting followed by direct acid leaching. A primary challenge in fluorocarbonate-bearing flowsheets is the generation of basic oxides, such as calcium oxide, during mineral decomposition, and calcium liberated during processing can co-precipitate REE into gypsum, reducing recovery (Dutrizac, 2017). The stoichiometric calcium inherently present in synchysite directly increases acid consumption and necessitates precise reagent control to prevent the precipitation of secondary phases, such as gypsum ($CaSO_4 \cdot 2H_2O$), which can severely blind downstream solid-liquid separation and solvent extraction circuits.

8. Conclusions

Quantitative process mineralogy is a foundational element of sustainable mining and mineral processing for critical metals. The case studies presented here support several general conclusions. Correct mineral identification is the first requirement, because metals are hosted by multiple minerals with different processing behaviour and some hosts carry penalty elements. Metal deportment, calculated from mineral mass and mineral chemistry, sets the theoretical recovery ceiling and locates losses and potential by-products. Liberation, association and exposure by size fraction define the grind target and the practical limits of physical separation, and the comparison of mineralogically derived grade-recovery curves against plant performance converts an unexplained shortfall into a specific, actionable diagnosis. Where liberation cannot account for a result, surface chemistry usually does. Mineralogy of leach residues explains hydrometallurgical behaviour that solution chemistry alone cannot.

Acquired early and interpreted with metallurgical intent, these data identify mineralogical barriers to recovery before capital is committed, enable selective mining and blending, guide comminution towards the necessary rather than the maximum degree of fineness, and support the characterisation and valorisation of waste streams. The value of an ore equals the recovery of that ore, and recovery is decided by mineralogy.

References

Aylmore, M.G., Merigot, K., Rickard, W.D.A., Evans, N.J., McDonald, B.J., Catovic, E., Spitalny, P. 2018. Assessment of a spodumene ore by advanced analytical and mass spectrometry techniques to determine its amenability to processing for the extraction of lithium. Minerals Engineering, 119, pp. 137–148

Ballantyne, G.R., Powell, M.S., 2014. Benchmarking comminution energy consumption for the processing of copper and gold ores. Minerals Engineering 65, 109–114.

Blannin, R., Frenzel, M., Tolosana-Delgado, R., Bachmann, K., Gomez Escobar, A., Pereira, L., Gutzmer, J., 2024. A quantitative particle-based approach for the geometallurgical assessment of tailings deposits. Earth Science, Systems and Society 4, 10102.

Berry, L., Agarwal, V., Galvin, J., and Safarzadeh, M. S. 2018. Decomposition of monazite concentrate in sulphuric acid. Canadian Metallurgical Quarterly, 57, 422–433. https://doi.org/10.1080/00084433.2018.1478490.

Butcher, A.R., Dehaine, Q., Menzies, A.H., Michaux, S.P., 2023. Characterisation of ore properties for geometallurgy. Elements 19, 352–358.

Chehreh Chelgani, S., 2013. Study on the surface chemistry behavior of pyrochlore during froth flotation. PhD thesis, The University of Western Ontario, London, Canada.

Chetty, D., Nwaila, G.T., Xakalashe, B., 2023. Fire and water: geometallurgy and extractive metallurgy. Elements 19, 365–370.

Demol, J., Ho, E., Soldenhoff, K., Karatchevtseva, I., and Senanayake, G. 2022. Beneficial effect of iron oxide/hydroxide minerals on sulfuric acid baking and leaching of monazite. *Hydrometallurgy*, *211*, 105864. https://doi.org/10.1016/j.hydromet.2022.105864

Di Feo, A., Sauber, M.E., Almusned, B., Hart, B., Grammatikopoulos, T., 2025. Impact of water recycling on spodumene losses during the mica flotation stage in lithium ore beneficiation. Minerals Engineering 234, 109773.

Dutrizac, J.E., 2017. The behaviour of the rare earth elements during gypsum ($CaSO_4 \cdot 2H_2O$) precipitation. Hydrometallurgy 174, 38–46.

Frenzel, M., Baumgartner, R., Tolosana-Delgado, R., Gutzmer, J., 2023. Geometallurgy: present and future. Elements 19, 345–351.

Gibson, C., 2016. The flotation of niobium oxide minerals from carbonatite ores. PhD thesis, Queen's University, Kingston, Canada.

Gibson, C., Aghamirian, M., Grammatikopoulos, T. 2017. The beneficiation of lithium minerals from hard rock deposits. Mining Engineering, 69(8), pp. 18-37.

Gillerman, V.S., Jercinovic, M.J, and Schmitz, M.D., 2025. Neodymium-Rich Monazite of the Lemhi Pass District, Idaho and Montana: Chemistry and Geochronology. Minerals, 15, 1156.

Grammatikopoulos, T., Aghamirian, M., Fedikow, F., Mayo, T., 2021. Mineralogical characterization and preliminary beneficiation of the Zoro Lithium Project, Manitoba, Canada. Mining, Metallurgy & Exploration 38, 329–346.

Grammatikopoulos, T., Downing, S., 2020. The disruptive role of process mineralogy in geology and the mineral processing industry. Aspects in Mining & Mineral Science 5, 571–579.

Grammatikopoulos, T., Mercer, W., Gunning, C., 2013. Mineralogical characterization using QEMSCAN of the Nechalacho heavy rare earth metal deposit, Northwest Territories, Canada. Canadian Metallurgical Quarterly 52, 265–277.

Grammatikopoulos, T., Glazier, R., Galenzoski, J., Grammatikopoulos, S., Dosbaba, M., Gugala E.P., and Joy, B., 2026. Fluorapatite as the Primary Rare Earth Element Host in the Hecla-Kilmer Alkaline Carbonatite Deposit, Northern Ontario, Canada: Mineralogical Controls, TIMA-X–Guided Microanalysis, and Implications for Rare Earth Processing. The 8th International Symposium on Process Mineralogy, Submitted.

International Energy Agency, 2025. Global Critical Minerals Outlook 2025. IEA, Paris.

Jordens, A., Sheridan, R.S., Rowson, N.A., Waters, K.E., 2014. Processing a rare earth mineral deposit using gravity and magnetic separation. Minerals Engineering 62, 9–18.

Opoku, P.A., Albijanic, B., Nikoloski, A.N., Tadesse, B., 2025. Surface chemistry modifications in grinding and flotation of spodumene. Minerals Engineering 234, 109676.

Pereira, L., Schach, E., Tolosana-Delgado, R., Frenzel, M., 2023. All about particles: modelling ore behaviour in mineral processing. Elements 19, 359–364.

da Silva, R.J.F., Dutra, A.J.B., Afonso, J.C., 2012. Alkali fusion followed by a two-step leaching of a Brazilian zircon concentrate. Hydrometallurgy 117–118, 93–100.

Su, A., Tian, W., Wang, Z., Wang, W. & Gong, T., 2025. Examining the quantification capability of automated mineralogy system: A machine learning approach. Journal of Geophysical Research: Machine Learning and Computation, 2, e2024JH000476. https://doi.org/10.1029/2024JH000476

Tusa, L., Frenzel, M., Pereira, L., Gutzmer, J., 2025. Geometallurgy: future directions. SEG Discovery.

Watari, T., Nansai, K., Nakajima, K., 2020. Review of critical metal dynamics to 2050 for 48 elements. Resources, Conservation and Recycling 155, 104669.

Watts, K.E., Andersen, A.K., 2025. Complex carbonate ore mineralogy in the Mountain Pass carbonatite rare earth element deposit, USA. American Mineralogist 110, doi:10.2138/am-2025-9822.

Xiao, Z., Zhang, W., 2024. Review of allanite: properties, occurrence and mineral processing technologies. Green and Smart Mining Engineering 1(1), 40–52.